Nanoscale Advances

ROYAL SOCIETY OF CHEMISTRY

PAPER

View Article Online
View Journal | View Issue

Cite this: *Nanoscale Adv.*, 2025, **7**, 2663

Nanomagnetic nickel complex based on salicylamide and L-proline ligands as an efficient heterogeneous catalyst for synthesis of tetrazoles

Chou-Yi Hsu,[a] Ghusoon Faidhi Hameed,[b] Irfan Ahmad,[c] Abhinav Kumar,*[dij] Subbulakshmi Ganesan,[e] Aman Shankhyan,[f] S. Sunitha[g] and Rajashree Panigrahi[h]

A novel salicylamide–L-proline–nickel(II) complex, supported on magnetic iron oxide [Fe_3O_4@salicylamide–L-proline–Ni(II)], was synthesized through a three-step procedure. This included the functionalization of Fe_3O_4 with amine groups using glycine as a linker, followed by direct amidation of salicylic acid and its subsequent coordination with Ni(II) and L-proline as a co-ligand to form the nanomagnetic Ni(II) complex. The resulting catalyst was comprehensively characterized by several techniques. The catalyst exhibited outstanding catalytic performance in the homoselective synthesis of 5-substituted-1*H*-tetrazoles from benzonitriles. Notably, it demonstrated excellent recyclability, maintaining high efficiency over eight reaction cycles. The use of a low-cost linker, ligand, and complex catalyst, combined with easy magnetic separation, minimal leaching, and scalability, renders this approach both environmentally sustainable and economically advantageous compared to traditional Ni-based methods.

Received 18th February 2025
Accepted 7th March 2025

DOI: 10.1039/d5na00168d

rsc.li/nanoscale-advances

1. Introduction

Azoles, a class of five-membered, nitrogen-containing heterocyclic compounds, represent a significant area of study within heterocyclic organic chemistry.[1] These aromatic parent structures, characterized by two double bonds, encompass a range of derivatives, including reduced analogs such as azolines and azolidines, which possess fewer nitrogen atoms. The number of nitrogen atoms within these heterocycles profoundly influences their chemical properties and diverse applications.[2–4] Ranging from one to five nitrogen atoms, these structures give rise to a variety of scaffolds, including pyrrole,[5] imidazole,[6] pyrazole,[7] triazole,[8] tetrazole, and pentazole.[9] Although pyrrole, imidazole, and pyrazole (containing one or two nitrogen atoms, respectively) occur naturally, azoles with more than two nitrogen atoms are predominantly synthetic and require laboratory synthesis.[10]

Tetrazole stands out among these as the aromatic five-membered organoheterocyclic compound with the highest nitrogen content (four nitrogen atoms and one carbon atom), making it a particularly noteworthy moiety in organic chemistry.[10] Pentazole, while possessing a higher nitrogen content, is not considered an organic molecule in the same way due to its lack of a carbon atom within the ring system.[9] Tetrazoles are versatile building blocks with diverse applications, notably in medicinal chemistry, but also in other fields like materials science and high-energy applications.[11–13] Due to the importance of these structures several synthetic procedures were provided for preparation of these materials from various synthons including nitriles, isocyanides, aldehydes, amines, and aryldiazonium salts.[10,14–19]

The synthesis of substituted tetrazoles from nitriles *via* [3 + 2] cycloaddition mechanism has garnered significant attention, evolving from traditional, metal-free approaches to more modern, metal-catalyzed methodologies.[20–26] While older methods often relied on elevated temperatures and solvents like DMF or toluene, sometimes incorporating catalysts such as triethylamine hydrochloride, iodine, or sulfamic acid, current research increasingly focuses on metal-catalyzed reactions. These modern methods, employing catalysts like palladium,[27]

[a]*Thunderbird School of Global Management, Arizona State University, Tempe Campus, Phoenix, Arizona 85004, USA*
[b]*Department of Chemistry, College of Education, University of Al-Qadisiyah, Iraq*
[c]*Department of Clinical Laboratory Sciences, College of Applied Medical Sciences, King Khalid University, Abha, Saudi Arabia*
[d]*Department of Nuclear and Renewable Energy, Ural Federal University Named after the First President of Russia Boris Yeltsin, Ekaterinburg 620002, Russia. E-mail: drabhinav@ieee.org*
[e]*Department of Chemistry and Biochemistry, School of Sciences, JAIN (Deemed to be University), Bangalore, Karnataka, India*
[f]*Centre for Research Impact & Outcome, Chitkara University Institute of Engineering and Technology, Chitkara University, Rajpura, Punjab, 140401, India*
[g]*Department of Chemistry, Sathyabama Institute of Science and Technology, Chennai, Tamil Nadu, India*
[h]*Department of Microbiology, IMS and SUM Hospital, Siksha 'O' Anusandhan (Deemed to be University), Bhubaneswar, Odisha-751003, India*
[i]*Department of Technical Sciences, Western Caspian University, Baku, Azerbaijan*
[j]*Refrigeration & Air-condition Department, Technical Engineering College, The Islamic University, Najaf, Iraq*

copper, indium,[28] silver,[29] neodymium,[30] erbium,[31] gadolinium,[32] samarium[33] and zinc, offer advantages such as milder reaction conditions including lower temperatures and shorter times. However, most of the reported methodologies use toxic solvents, expensive catalysts, high temperature and pressure, and harsh reaction conditions. As a result, these processes generate significant toxic waste, harming the environment and human health. This has led to stricter regulations and a push for green chemistry, which reduces waste and improves efficiency, but further catalyst development is still needed.

In accordance with the green chemistry principles, heterogeneous supported catalysts offer a compelling strategy for enhancing catalytic activity, promoting recyclability, and minimizing waste generation.[34–36] The integration of such catalysts with magnetic nanoparticles (MNPs) presents a particularly attractive avenue, affording not only improved catalytic performance but also facile separation and recovery.[37–41] MNPs have attracted considerable interest due to their inherent stability and the ease of manipulation *via* external magnetic fields.[37,42–44] The judicious combination of MNPs with catalytically active complexes, particularly those derived from sustainable and cost-effective precursors, results in a robust heterogeneous catalytic system.[45–47] This synergistic approach confers several distinct advantages, including a high surface area, excellent catalytic activity, simplified separation, and demonstrable reusability.[44,48] Consequently, such hybrid materials provide a promising platform for diverse applications in catalysis and chemical synthesis.[49]

To date, various nanomagnetic catalysts have been utilized for the synthesis of 5-substituted-1*H*-tetrazoles. However, many of these catalysts rely on toxic and expensive linkers, ligands, and metals, often requiring multi-step immobilization processes and harsh reaction conditions, Therefore, a greener approach is needed. To address this challenge, we explore a novel approach using glycine as a safe and affordable amine linker, salicylic acid and L-proline as green ligands, and nickel as an inexpensive and environmentally friendly metal center. The resulting nanocomposite effectively immobilizes the nickel catalytic species, and the supported Ni complex demonstrates high catalytic efficiency for the synthesis of 5-substituted-1*H*-tetrazoles under environmentally benign conditions.

2. Experimental

2.1. Materials and instruments

All chemicals and solvents were purchased from Merck Millipore and Sigma-Aldrich and used as received. Reactions were monitored by thin-layer chromatography (TLC) on commercial glass-backed plates, with spot visualization under UV light at 254 nm. Fourier transform infrared (FT-IR) spectra were recorded using a PerkinElmer 597 spectrophotometer with KBr plates. X-ray powder diffraction (XRD) analysis was carried out using a PHILIPS PW1730 powder diffractometer with Cu Kα radiation (λ = 1.54056 Å). Inductively Coupled Plasma Optical Emission Spectroscopy (ICP-OES) was performed using a Varian Vista Pro Analyzer. Energy-dispersive X-ray (EDX) and EDX mapping analyses were performed using a TESCAN VEGA 3 scanning electron microscope (SEM). Transmission electron microscopy (TEM) images were obtained using a CM120 microscope. The magnetic properties of the sample were analyzed using Vibrating Sample Magnetometry (VSM) analysis *via* a VSM-250 (YP, Jilin, China). Brunauer–Emmett–Teller (BET) analysis was performed using a TriStar 3020 analyzer.

2.2. Typical procedure for synthesis of [Fe_3O_4@salicylamide–L-proline–Ni(II)] nanocomposite

Fe_3O_4 MNPs were prepared according to a previously reported procedure.[50] Subsequently, 10 g of Fe_3O_4 MNPs were dispersed in 200 mL of a 1 : 1 (v/v) ethanol/water mixture and sonicated for 60 minutes. Then 50 mL aqueous solution of 0.5 M glycine (1.88 g) was then added dropwise to the suspension under vigorous stirring. The resulting mixture was refluxed under a nitrogen atmosphere with vigorous stirring for 48 hours. After the completion of reaction, the obtained Fe_3O_4@Gly MNPs were magnetically separated, washed sequentially with hot water and ethanol, and dried in vacuum oven at 80 °C for 24 h. In the subsequent modification step, 5 g of the Fe_3O_4@Gly MNPs were dispersed in 100 mL of dry toluene through sonication for 1 h to form a uniform suspension. Then a mixture of 2.06 g dicyclohexylcarbodiimide (DCC) (10 mmol), 1.38 g salicylic acid (10 mmol), and 5 mL of pyridine was then added to this suspension. The reaction mixture was first stirred at room temperature for 2 hours, followed by reflux under a nitrogen atmosphere for 48 h. The resulting Fe_3O_4@salicylamide product was then isolated magnetically, washed sequentially with hot ethanol and water, and dried at 80 °C for 4 h. Finally, 5 g of Fe_3O_4@salicylamide was dispersed in a 1 : 1 water–ethanol mixture (150 mL) for 30 minutes. To this suspension, 2.488 g $Ni(OAc)_2 \cdot 4H_2O$ (10 mmol), 1.15 g L-proline (10 mmol) and five drops of triethylamine were introduced. The reaction mixture was refluxed for 24 hours. The [Fe_3O_4@salicylamide–L-proline–Ni(II)] nanocomposite was then magnetically separated, washed with hot water and ethanol, and dried at 80 °C for 6 hours.

2.3. General procedure for synthesis of 5-substituted-1*H*-tetrazoles catalyzed by [Fe_3O_4@salicylamide–L-proline–Ni(II)] nanocomposite

A mixture of aryl nitrile (1.0 mmol), sodium azide (1.3 mmol), and the [Fe_3O_4@salicylamide–L-proline–Ni(II)] nanocomposite catalyst (5 mg) was added to a round-bottom flask containing 3 mL of PEG-400. The reaction mixture was stirred at 120 °C until completion, as determined by thin-layer chromatography (TLC). Upon completion, the reaction mixture was diluted with hot water, and the catalyst was magnetically separated. The resulting aqueous solution was acidified to pH ~ 1 with 2 N hydrochloric acid and subsequently extracted with ethyl acetate. The combined organic extracts were dried over anhydrous sodium sulfate, filtered, and concentrated under reduced pressure. The crude product was purified by column chromatography on silica gel using a petroleum ether/ethyl acetate mixture as the eluent.

3. Results and discussions

In this study, a novel nickel complex was successfully immobilized on Fe_3O_3 MNPs through an initial amine functionalization step using glycine as an inexpensive and environmentally friendly linker. Salicylic acid, a cost-effective ligand compared to aldehydes and ketones, was then grafted onto the MNPs surface through direct amidation with the surface amine groups. This heterostructure was subsequently used to coordinate with nickel(II) acetate tetrahydrate and L-proline as an efficient co-ligand, resulting in the formation of a six-coordinated nickel(II) complex. This strategy provides an effective nanomagnetic electron donor environment for nickel complexation (Scheme 1). The synthesis and immobilization of the targeted complex were thoroughly monitored and confirmed through various techniques, including FT-IR, XRD, TGA, EDX, ICP-OES, elemental mapping, FE-SEM, TEM, and VSM, to assess their structural and magnetic properties.

3.1. Catalyst characterization

The FTIR spectra of pristine Fe_3O_4, Fe_3O_4@Gly, Fe_3O_4@salicylamide, and the [Fe_3O_4@salicylamide–L-proline–Ni(II)] nanocomposite are presented in Fig. 1. The FTIR spectrum of pristine Fe_3O_4 displays an Fe–O stretching band at 564 cm^{-1}, while the functionalized samples show this band shifted to the range of 555–558 cm cm^{-1}. The broad peaks observed between 3200 and 3600 cm cm^{-1} and at 1624 cm cm^{-1} correspond to the O–H bond vibrations of hydroxyl groups on the Fe_3O_4 surface. In the FTIR spectrum of Fe_3O_4@Gly, additional peaks are observed at 3488, 3434, 2973, 2920, 1629, 1303, and 1100 cm^{-1}. These peaks are attributed to the stretching vibrations of NH_2, aliphatic C–H, and carboxylate groups, respectively, providing clear evidence of successful functionalization with glycine. The FTIR spectrum of Fe_3O_4@salicylamide displays new peaks at 3132 and 3044 cm^{-1}, which are assigned to the N–H stretching vibration of the amide group and the aromatic C–H stretching vibration. The band at 1705 cm^{-1} corresponds to the carbonyl stretching vibration, while aromatic C–C stretching vibrations are observed at 1595 and 1487 cm^{-1}. An Ar–O stretching vibration is observed at 1250 cm^{-1}, further supporting successful modification of the Fe_3O_4 surface with salicylamide. The FTIR spectrum of the [Fe_3O_4@salicylamide–L-proline–Ni(II)]

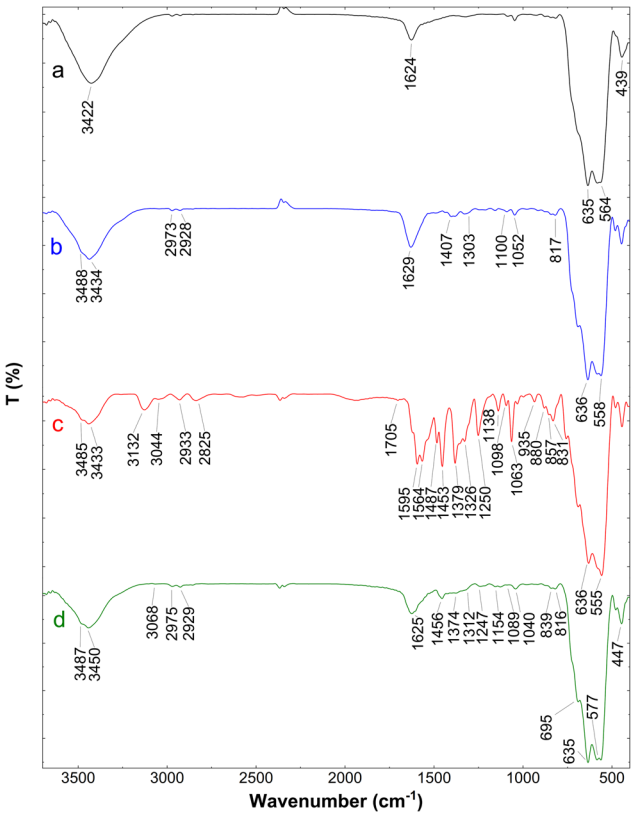

Fig. 1 FT-IR analysis of (a) Fe_3O_4, (b) Fe_3O_4@Gly (c) Fe_3O_4@salicylamide and (d) [Fe_3O_4@salicylamide–L-proline–Ni(II)] nanocomposite.

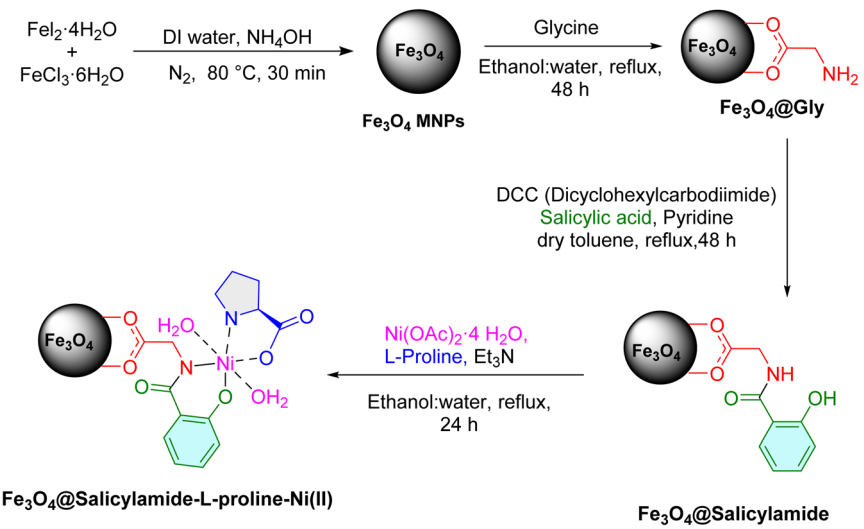

Scheme 1 Stepwise synthesis of [Fe_3O_4@salicylamide–L-proline–Ni(II)] nanocomposite.

nanocomposite reveals a peak at 1154 cm^{-1}, indicating the presence of L-proline in the complex.[51] The incorporation of Ni(II) was confirmed through EDX, ICP, and elemental mapping analyses, providing additional validation of the successful synthesis of the complex and the presence of Ni.

Powder X-ray diffraction (P-XRD) analysis was used to examine the crystalline structure of the [Fe_3O_4@salicylamide–L-proline–Ni(II)] nanocomposite. The resulting diffraction pattern displayed sharp peaks at 2θ values of 30.34°, 35.64°, 43.24°, 53.79°, 57.14°, and 62.94°, corresponding to the (220), (311), (400), (422), (511) and (440) lattice planes of Fe_3O_4. The observed diffraction pattern closely matched the characteristic peaks of Fe_3O_4 MNPs (JCPDS 88-0866),[52] further verifying that the Fe_3O_4 crystalline phase was maintained throughout the functionalization process Fig. 2.

The thermal stability of the [Fe_3O_4@salicylamide–L-proline–Ni(II)] nanocomposite was assessed using TGA analysis (Fig. 3). A weight loss of approximately 4.2% observed below 200 °C is attributed to the removal of physisorbed moisture and solvents. A second, more substantial weight loss of about 14% occurs between 200 and 600 °C, corresponding to the degradation of the salicylamide and L-proline organic components on the catalyst surface throught the pyrolysis reaction. These findings confirm the presence of organic moieties on the catalyst surface and indicate its thermal stability up to 200 °C, suggesting its suitability for reactions conducted at temperatures below this limit.

The chemical composition of the synthesized [Fe_3O_4@salicylamide–L-proline–Ni(II)] nanocomposite was examined using energy dispersive spectroscopy (EDS) (Fig. 4). The analysis revealed peaks corresponding to iron (55.21 wt%, 26.23 at%) and oxygen (22.63 wt%, 37.51 at%), confirming their presence as integral components of the Fe_3O_4 structure. Additionally, the detection of carbon (11.97 wt%, 26.47 at%) and nitrogen (3.57 wt%, 6.77 at%) peaks indicates the successful incorporation of organic linkers and ligands on the surface of Fe_3O_4. The observed nickel (6.62 wt%, 2.98 at%) peak further confirms the presence of nickel complexed with the ligands on the surface of the magnetic nanoparticles (MNPs). Additionally, ICP-OES analysis revealed that the nickel content in the [Fe_3O_4@salicylamide–L-proline–Ni(II)] nanocomposite was approximately 1.17 × 10^{-3} mol g^{-1}.

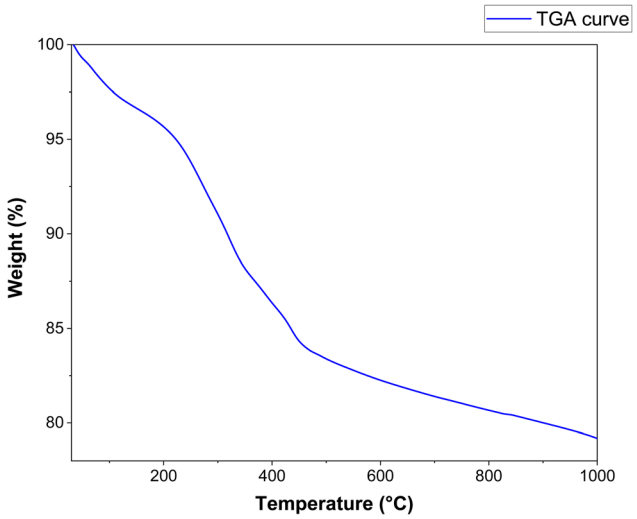

Fig. 3 TGA analysis of [Fe_3O_4@salicylamide–L-proline–Ni(II)] nanocomposite.

The elemental mapping images (Fig. 5) show that the surface of the [Fe_3O_4@salicylamide–L-proline–Ni(II)] nanocomposite is predominantly made up of iron and oxygen, which originate from the magnetic support. Additionally, carbon, nitrogen, and nickel are present in lower amounts but are evenly distributed across the surface. This indicates that the ligands and complexes are securely attached to the surface, ensuring that guest reactants can easily access the active sites.

The morphology of the synthesized [Fe_3O_4@salicylamide–L-proline–Ni(II)] nanocomposite was investigated using scanning electron microscopy (SEM) analysis (Fig. 6). The SEM images show spherical shape crystallites arranged in a well-dispersed

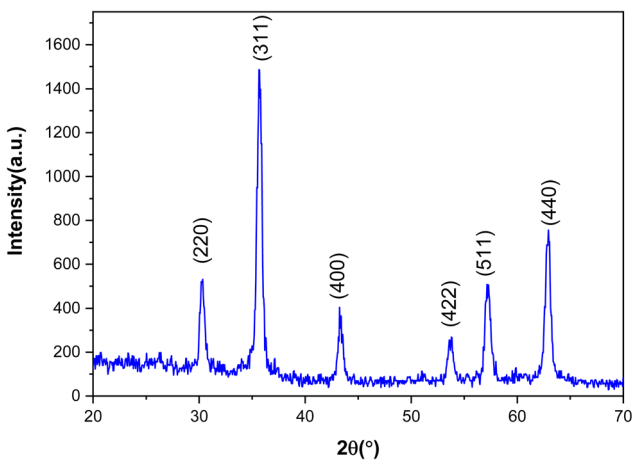

Fig. 2 XRD analysis of [Fe_3O_4@salicylamide–L-proline–Ni(II)] nanocomposite.

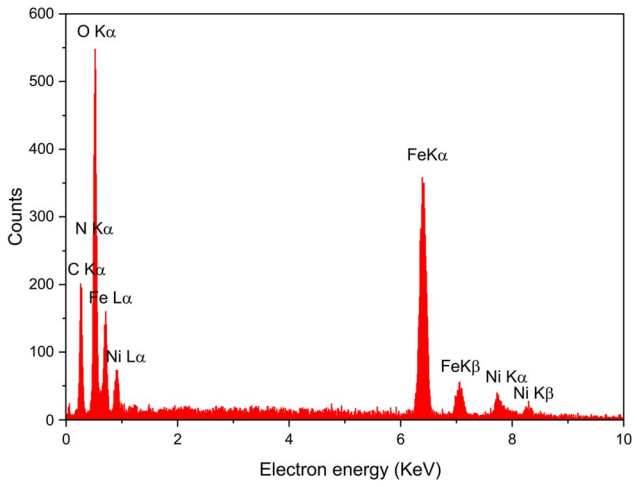

Fig. 4 EDAX analysis of [Fe_3O_4@salicylamide–L-proline–Ni(II)] nanocomposite.

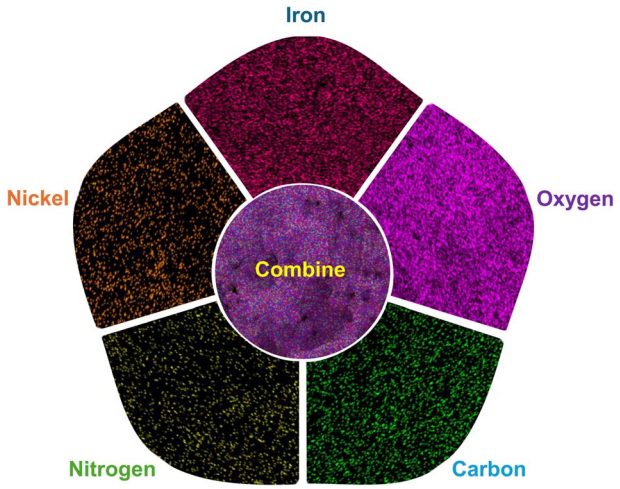

Fig. 5 EDX elemental mapping images of [Fe_3O_4@salicylamide–L-proline–Ni(II)] nanocomposite.

manner. The overall surface morphology exhibits the characteristic features of iron oxide nanoparticles, confirming their stability throughout the post-synthetic modification process.[53] While some degree of agglomeration is observed, it is likely attributed to the surface modification, which further supports the successful synthesis of the target catalyst.

The TEM micrographs of the [Fe_3O_4@salicylamide–L-proline–Ni(II)] nanocomposite clearly depict a spherical morphology, with particle sizes ranging from 14 to 25 nm and a uniform dispersion. These images reveal distinct surface characteristics, further confirming the successful immobilization of the targeted complex onto the MNPs support (Fig. 7).

Fig. 8 displays the magnetization curves of the prepared samples at room temperature. The saturation magnetization (M_s) values for bare Fe_3O_4, as well as for the synthesized Fe_3O_4@Gly, Fe_3O_4@salicylamide, and [Fe_3O_4@salicylamide–L-proline–Ni(II)] nanocomposite, were approximately 60.97, 47.31, 41.02, and 29.96 emu g^{-1}, respectively. The reduction in M_s for each functionalized MNPs can be attributed to the increased sample mass caused by the incorporation of diamagnetic organic ligands, which weaken the magnetic properties of the Fe_3O_4 core. Nevertheless, the complex still retains notable magnetic properties, making it well-suited for various magnetically guided applications.

To analyze the porous structure of the [Fe_3O_4@salicylamide–L-proline–Ni(II)] nanocomposite, N_2 physisorption was used.

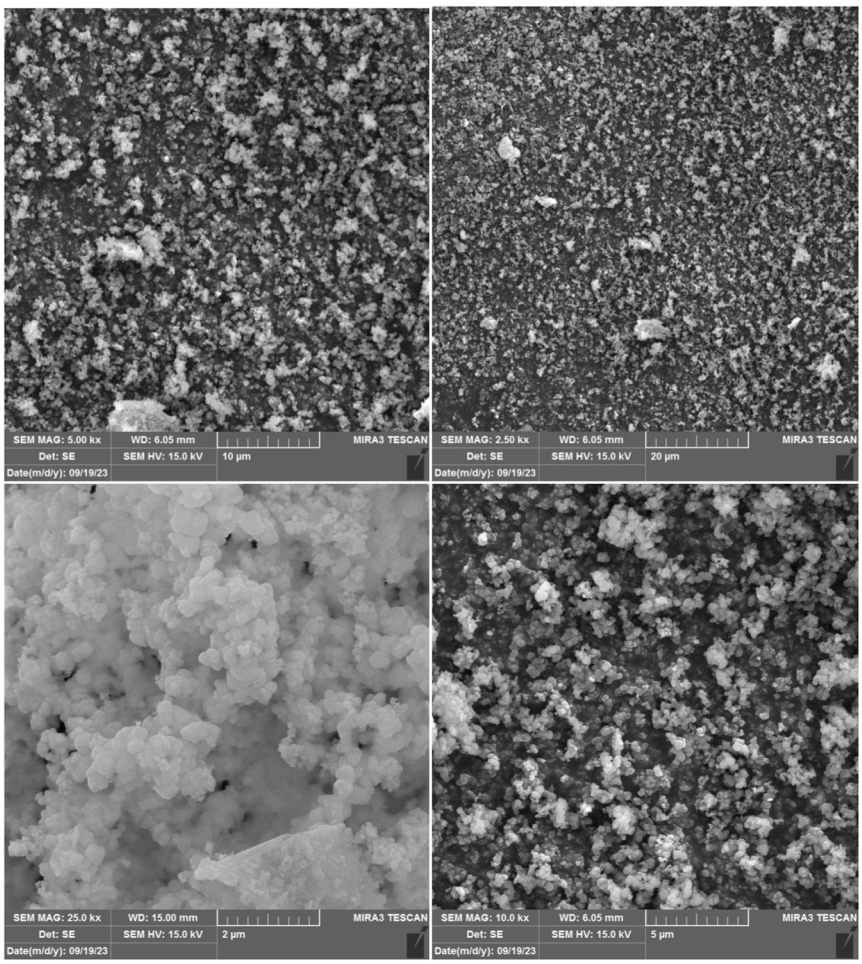

Fig. 6 SEM images of [Fe_3O_4@salicylamide–L-proline–Ni(II)] nanocomposite.

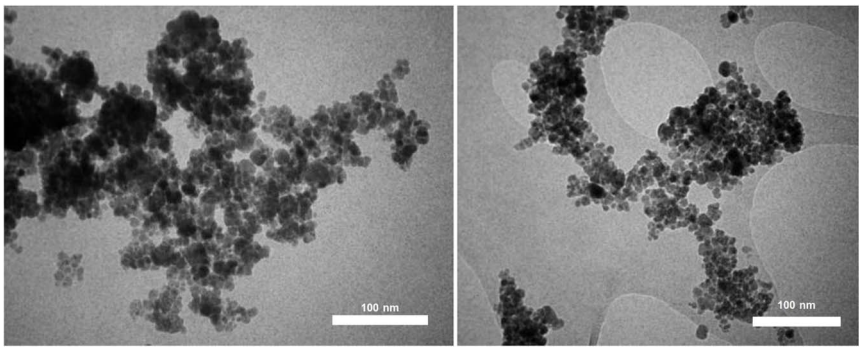

Fig. 7 TEM images of [Fe_3O_4@salicylamide–L-proline–Ni(II)] nanocomposite.

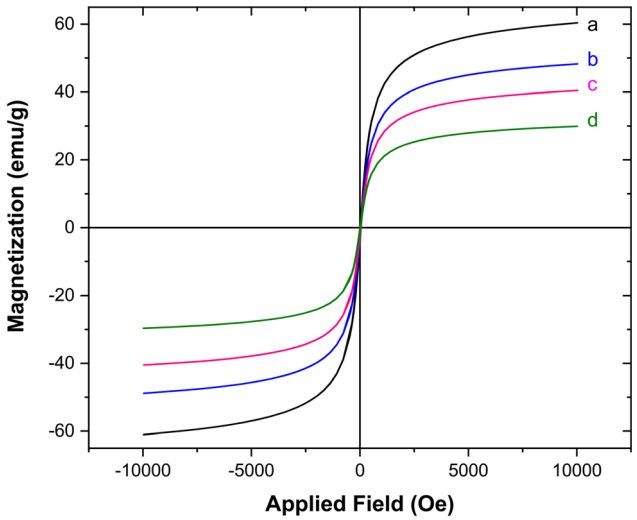

Fig. 8 VSM analysis of (a) Fe_3O_4, (b) Fe_3O_4@Gly, (c) Fe_3O_4@-salicylamide and (d) [Fe_3O_4@salicylamide–L-proline–Ni(II)] nanocomposite.

The resulting type IV isotherms with a noticeable hysteresis loop suggest a mesoporous character, which was further supported by a pore diameter of about 42.168 nm and a total pore volume of 0.098 $cm^3\ g^{-1}$. The calculated specific surface area of 47.55 $m^2\ g^{-1}$ is lower than that of pure Fe_3O_4 (72.148 $m^2\ g^{-1}$),[54] likely due to pore obstruction and cavity filling during the functionalization process (Fig. 9).

3.2. Catalytic study

After thoroughly characterizing the [Fe_3O_4@salicylamide–L-proline–Ni(II)] nanocomposite, we investigated its catalytic activity in various organic reactions, including the synthesis of tetrazoles. In the first stage, we optimized key reaction parameters such as catalyst loading, solvent, and temperature (Table 1). The optimization was carried out using the [Fe_3O_4@-salicylamide–L-proline–Ni(II)] nanocomposite as the catalyst in a model reaction involving 1 mmol of benzonitrile and 1.3 mmol of sodium azide. Initially, the reaction was conducted without a catalyst, yielding no conversion (Table 1, entry 1). When the reaction was performed in PEG-400 under reflux, varying amounts of catalyst were tested, and a significant improvement in yield was observed (Table 1, entries 2–5). A catalyst loading of 1 mg resulted in a low yield (Table 1, entry 2), while increasing the catalyst amount to 5 mg led to an excellent product yield (Table 1, entry 5). However, further increasing the catalyst loading to 7 mg did not enhance the yield or reduce the reaction time (Table 1, entry 6). Subsequently, various green solvents, including water, ethanol and their mixture (1 : 1), were also tested, but none produced satisfactory results (Table 1, entries 7 and 8). Furthermore, reducing the reaction temperature to 80 °C or room temperature resulted in only moderate or negligible product formation, respectively (Table 1, entries 10 and 11). The influence of sodium azide stoichiometry on reaction efficacy was subsequently examined (Table 1, entries 12 and 13). Quantification of product yields revealed that an

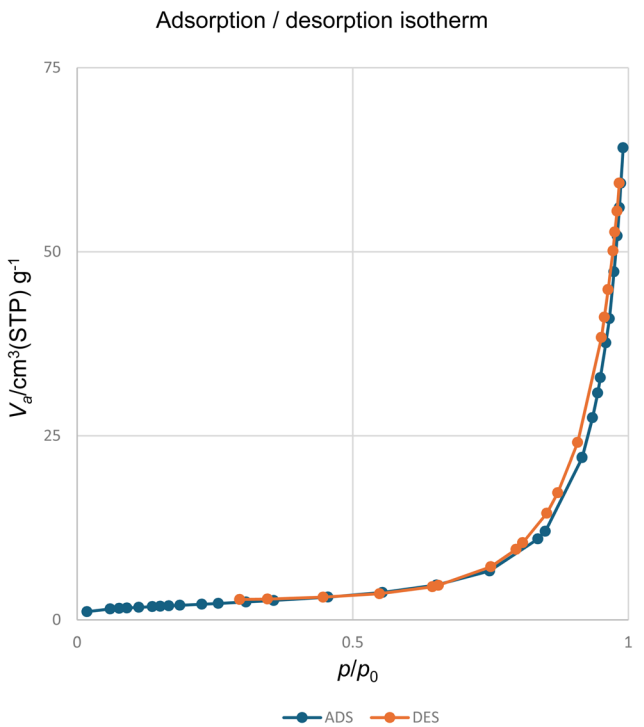

Fig. 9 N_2 adsorption–desorption isotherm of [Fe_3O_4@salicylamide–L-proline–Ni(II)] nanocomposite.

Table 1 Optimization of synthesis of 5-phenyl-1*H*-tetrazol in the presence of [Fe_3O_4@salicylamide–L-proline–Ni(II)] complex

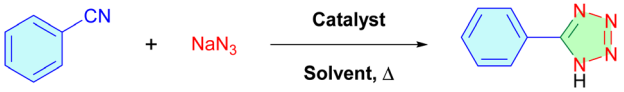

Entry	Catalyst	Catalyst amount (mol%)	Solvent	Temperature (°C)	Time (min)	Yield[a,b] (%)
1	[Fe_3O_4@salicylamide–L-proline–Ni(II)]	—	PEG-400	120	1 day	NR
2	[Fe_3O_4@salicylamide–L-proline–Ni(II)]	1	PEG-400	120	90	36
3	[Fe_3O_4@salicylamide–L-proline–Ni(II)]	2	PEG-400	120	50	69
4	[Fe_3O_4@salicylamide–L-proline–Ni(II)]	4	PEG-400	120	30	92
5	[Fe_3O_4@salicylamide–L-proline–Ni(II)]	5	PEG-400	120	25	97
6	[Fe_3O_4@salicylamide–L-proline–Ni(II)]	7	PEG-400	120	25	97
7	[Fe_3O_4@salicylamide–L-proline–Ni(II)]	5	Water	Reflux	180	45
8	[Fe_3O_4@salicylamide–L-proline–Ni(II)]	5	Ethanol	Reflux	135	73
9	[Fe_3O_4@salicylamide–L-proline–Ni(II)]	5	Water : ethanol (1 : 1)	Reflux	30	64
10	[Fe_3O_4@salicylamide–L-proline–Ni(II)]	5	PEG-400	80	2 h	51
11	[Fe_3O_4@salicylamide–L-proline–Ni(II)]	5	PEG-400	r.t.	6 h	Trace
12	[Fe_3O_4@salicylamide–L-proline–Ni(II)]	5	PEG-400	120	25	97[c]
13	[Fe_3O_4@salicylamide–L-proline–Ni(II)]	5	PEG-400	120	25	94[d]
14	Fe_3O_4	5	PEG-400	120	120	Trace
15	Fe_3O_4@Gly	5	PEG-400	120	120	Trace
16	Fe_3O_4@salicylamide	5	PEG-400	120	120	Trace

[a] Isolated yield. [b] Conditions: benzonitrile (1 mmol), sodium azide (1.2 mmol), [Fe_3O_4@salicylamide–L-proline–Ni(II)] catalyst (mg) and solvent (3 mL). [c] The reaction was carried out with 1.4 mmol of NaN_3. [d] The reaction was carried out with 1 mmol of NaN_3.

increase in NaN_3 from 1.2 mmol to 1.4 mmol did not significantly enhance reaction performance. Conversely, a reduction to 1.0 mmol resulted in a demonstrable decrease in yield. Furthermore, to elucidate the catalytic role of the Ni species, a comparative study was conducted utilizing various catalyst intermediates: bare Fe_3O_4, Fe_3O_4@Gly, and Fe_3O_4@salicylamide (Table 1, entries 14–16). These intermediates yielded only trace amounts of the desired product, underscoring the indispensable contribution of the nickel(II) component in achieving optimal catalytic activity for the [Fe_3O_4@salicylamide–L-proline–Ni(II)] catalyst.

Overall, the optimal conditions were found to be 5 mg of the [Fe_3O_4@salicylamide–L-proline–Ni(II)] catalyst in PEG-400 at 120 °C, which yielded the best results for the synthesis of 5-substituted 1*H*-tetrazoles.

The scope and efficiency of the optimized methodology was evaluated in various substrates including substituted benzonitriles, as well as different aliphatic cyano compounds (Table 2). The results revealed that all substrates reacted effectively, yielding the desired tetrazoles in good to excellent amounts. The electron-withdrawing groups on the aryl ring increased reactivity, while electron-donating groups had the opposite effect. Moreover, the reaction was successfully applied to aliphatic nitriles, leading to the formation of the desired tetrazoles with yields reaching up to 90%. Additionally, the reaction of dicyanoarenes including; phthalonitrile, isophthalonitrile, and terephthalonitrile derivatives (Table 2 entries 5–7), with a stoichiometric equivalent of azide reagent afforded the desired 2-(1*H*-tetrazol-5-yl)benzonitrile derivative as the sole product. The observed retention of the second cyano substituent demonstrates the remarkable homoselectivity of this catalytic methodology for the synthesis of 5-substituted tetrazoles. Finally, a 10-fold scale-up of the reaction, using benzonitrile as a model reaction maintaining stoichiometric ratios, yielded 94% of the desired product in 35 min, demonstrating the method's feasibility for gram-scale production. This efficient and rapid transformation confirms the method's potential for industrial application in 5-substituted 1*H*-tetrazole synthesis.

The plausible mechanism for the catalytic cycle in the synthesis of 5-aryl-1*H*-tetrazoles, facilitated by the [Fe_3O_4@salicylamide–L-proline–Ni(II)] nanocomposite, is outlined in Scheme 2. In the first step, the Ni(II) center interacts with the sodium azide salt (NaN_3), generating a reactive nitrogen species. This intermediate then reacts with an organic nitrile (R–CN) on the catalyst surface. The interaction between the intermediate and the Ni complex induces the subsequent ring closure, resulting in the formation of the tetrazole structure. The cycle concludes with the regeneration of the catalyst, making it ready for the next catalytic iteration.[65]

3.3. Reusability of catalyst

The ability to recycle a catalyst from the reaction medium is a powerful characteristic that makes it particularly valuable for catalysis applications, especially from an environmental perspective.[66] In this regard, we investigated the model reaction under optimized conditions for the synthesis of 5-phenyl-1*H*-tetrazole derivatives. After the reaction reached completion, as indicated in Table 2, the reaction was stopped, and the catalyst was separated following the procedure outlined in the

Table 2 The scope of synthesis of 5-substituted 1*H*-tetrazoles catalyzed by [Fe_3O_4@salicylamide–L-proline–Ni(II)] nanocomposite

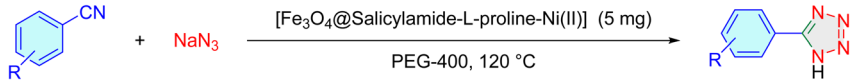

Entry	Aryl nitrile	Product	Time (min)	Yield[a,b] (%)	TON	TOF (min^{-1})	Melting point [ref.]
1	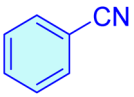	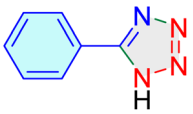	25	97	16 440	657	218–220 (ref. 55)
2	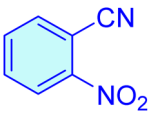	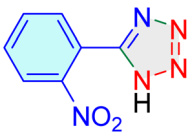	20	95	16 101	805	159–161 (ref. 56)
3	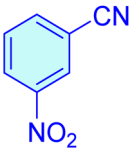	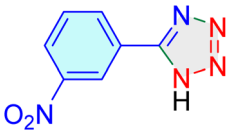	25	97	16 440	657	155–156 (ref. 55)
4	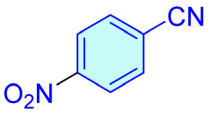	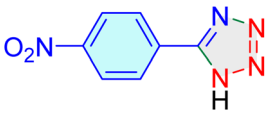	15	99	16 779	1118	219–221 (ref. 55)
5	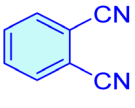	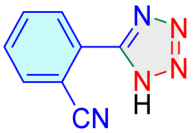	20	92	15 593	779	209–212 (ref. 57)
6	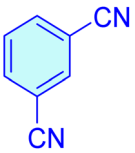	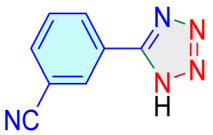	27	96	16 271	602	210–212 (ref. 57)
7	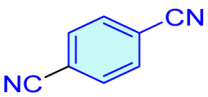	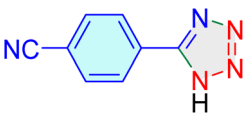	18	98	16 610	922	251–254 (ref. 57)
8	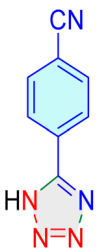	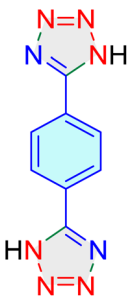	30	88	14 915	497	295–296 (ref. 58)
9	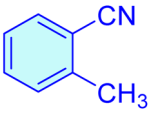	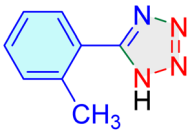	40	93	15 762	394	152–154 (ref. 59)
10	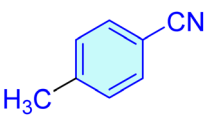	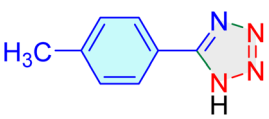	28	96	16 271	581	249–251 (ref. 55)

Table 2 (*Contd.*)

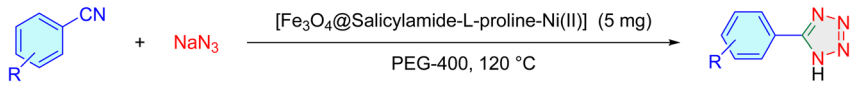

Entry	Aryl nitrile	Product	Time (min)	Yield[a,b] (%)	TON	TOF (min^{-1})	Melting point [ref.]
11	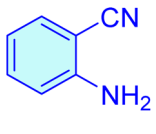	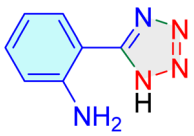	85	88	14 915	175	222–224 (ref. 60)
12	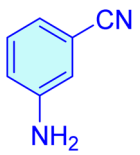	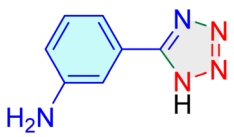	45	95	16 101	537	200–204 (ref. 61)
13	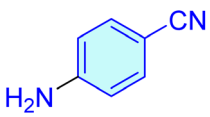	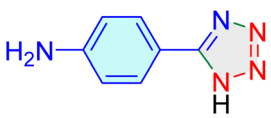	80	91	15 423	192	266–269 (ref. 55)
14	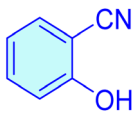	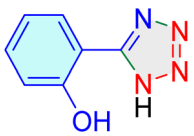	80	89	15 084	188	225–227 (ref. 62)
15	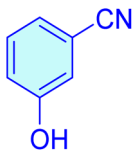	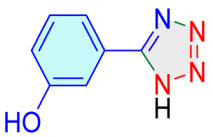	37	95	16 101	435	244–246 (ref. 63)
16	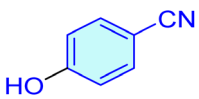	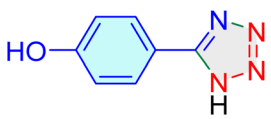	80	92	15 593	194	231–234 (ref. 55)
17	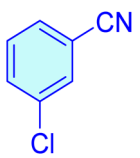	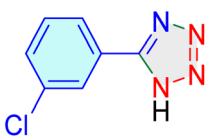	30	97	16 440	548	140–143 (ref. 64)
18	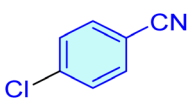	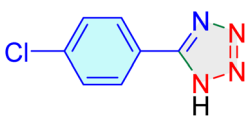	25	97	16 440	657	154–155 (ref. 55)

[a] Isolated yield. [b] Conditions: aryl nitrile (1.0 mmol), sodium azide (1.2 mmol) and [Fe_3O_4@salicylamide–L-proline–Ni(II)] complex (5 mol%) in PEG-400 (2 mL) at 120 °C.

Experimental section. It was then washed several times with ethyl acetate (EtOAc), water, and ethanol, before being dried in an oven at 80 °C. The recovered catalyst was subsequently reused in the next reaction cycle. The results demonstrate excellent reusability, with only a negligible loss in efficiency over eight consecutive reaction cycles (Fig. 10). These findings confirm the reusability and recyclability of the prepared catalyst under the optimized conditions.

To evaluate the stability of the [Fe_3O_4@salicylamide–L-proline–Ni(II)] nanocomposite following recyclability experiments, FT-IR, VSM and ICP-OES analyses were performed. The consistent FT-IR pattern observed after eight cycles (Fig. 11)

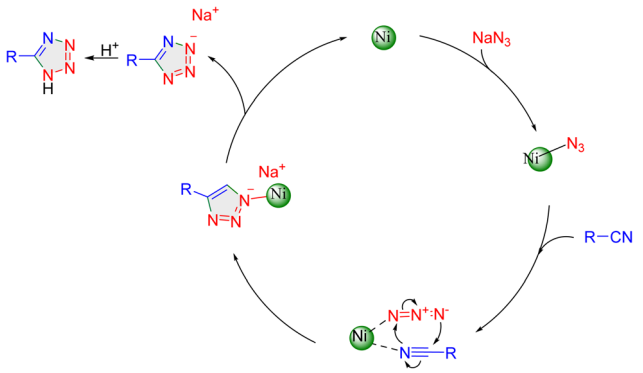

Scheme 2 Possible mechanism for synthesis of 5-substituted-1*H*-tetrazoles over the catalysis of [Fe_3O_4@salicylamide–L-proline–Ni(II)] nanocomposite.

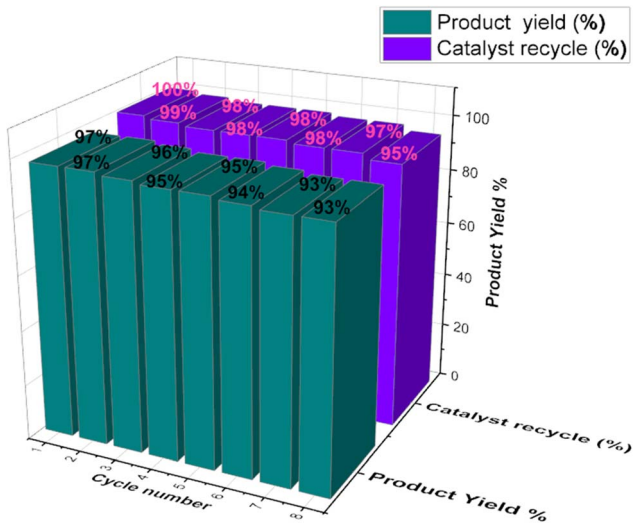

Fig. 10 The reusability of [Fe_3O_4@salicylamide–L-proline–Ni(II)] nanocomposite in the model reaction of 5-phenyl-1*H*-tetrazole synthesis.

demonstrates the exceptional chemostability and recyclability of the catalyst. Additionally, the M_s value of the recycled [Fe_3O_4@salicylamide–L-proline–Ni(II)] catalyst was determined to be 26.37 emu g^{-1} (Fig. 12). A comparative analysis with the fresh catalyst demonstrated only a modest reduction of 3.59 emu g^{-1} in the M_s value following eight recycling cycles. This observation indicates a high degree of magnetic stability, confirming that the material maintains sufficient magnetic responsiveness for effective separation *via* neodymium magnets. Finally, the ICP-OES results show that the Ni content in the recycled catalyst is nearly identical to that of the fresh catalyst (1.16×10^{-3} mol g^{-1}), indicating no significant metal leaching from the catalyst surface during the reaction cycles.

3.4. Leaching and hot filtration test

The nature of the catalytic species and their potential leaching into the reaction medium was examined using a hot filtration test and instrumental analysis. For this investigation, the model

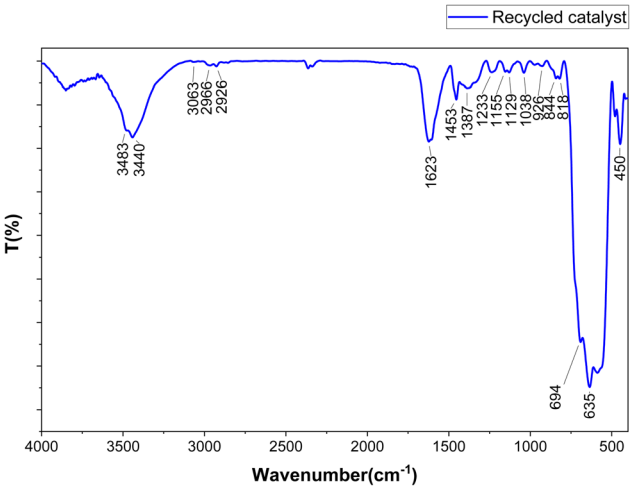

Fig. 11 FT-IR analysis of recovered [Fe_3O_4@salicylamide–L-proline–Ni(II)] nanocomposite.

reaction for synthesizing 5-phenyl-1*H*-tetrazole was selected. At the halfway point of the reaction, the [Fe_3O_4@salicylamide–L-proline–Ni(II)] nanocomposite was magnetically separated from the reaction mixture (with a product yield of 67% at this time), and the reaction was allowed to proceed for an additional half of the reaction time. The results revealed that the product yield increased by only a negligible 2% after catalyst removal, confirming the catalyst's predominantly heterogeneous nature. In addition, the ICP-OES analysis of the filtrate showed no trace of nickel, suggesting that there was very little metal leaching throughout the reaction.

3.5. Comparison study of catalytic activity

In recent years, several catalytic methods have been developed for synthesizing 5-aryl-1*H*-tetrazoles, given the significant importance of these compounds. However, a comparison between the catalytic performance of the [Fe_3O_4@salicylamide–

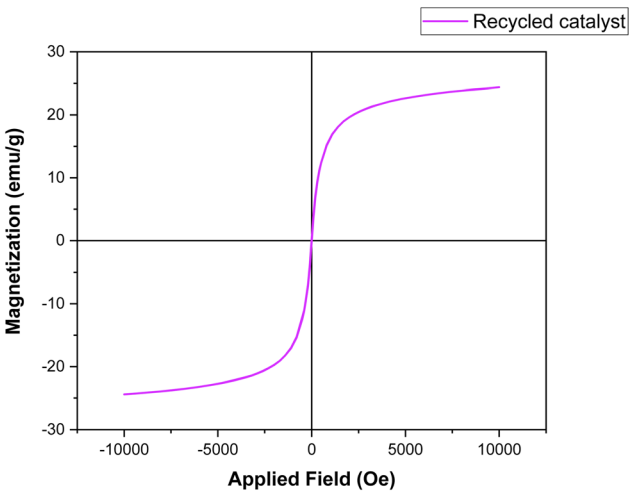

Fig. 12 VSM analysis of recovered [Fe_3O_4@salicylamide–L-proline–Ni(II)] nanocomposite.

Table 3 Comparison the [Fe_3O_4@salicylamide–L-proline–Ni(II)] nanocomposite catalytic activity in synthesis of 5-phenyl-1*H*-tetrazole model reaction

Entry	Catalyst (active site)	Time (min)	Isolated yield (%)	Reference
1	Fe_3O_4@L-lysine–Pd(0) (palladium)	60	99	27
2	[Fe_3O_4@TAM–Schiff-base–$Cu^{(II)}$] (copper)	100	98	68
3	Fe_3O_4@SiO_2@SBA-3@2-ATP–Cu (copper)	65	94	69
4	Co-$(PYT)_2$@BNPs (cobalt)	120	98	70
5	CF/MC/HA/A (silver)	10	93	29
6	Ag NPs (silver)	3 h	88	71
7	$CoFe_2O_4$@amino glycol/Gd (gold)	10	97	32
8	AuNPs (gold)	30 min	95	72
9	MCM-41@serine/Er (erbium)	10	96	31
10	MCM-41/3,4,5-tri-hydroxyphenyl acetic acid/Sm (samarium)	20	92	33
11	$InCl_3$ (indium)	15 h	92	28
12	Nd–Schiff-base@BMNPs (neodymium)	3 h	98	30
13	Polymer-bound $AlCl_3$ (aluminium)	6 h	79	20
14	SSA (sulfuric acid)	4 h	88	67
15	[Fe_3O_4@salicylamide–L-proline–Ni(II)] (nickel)	25	97	This work

L-proline–Ni(II)] nanocomposite and the most efficient green methods in the literature reveals several limitations of the latter. While previous catalysts often suffer from issues like high costs (especially for precious metals such as palladium, indium,[28] silver,[29] neodymium,[30] erbium,[31] gadolinium,[32] and samarium[33]), the need for harsh acidic conditions,[67] long reaction times, and toxic reagents or solvents, the [Fe_3O_4@-salicylamide–L-proline–Ni(II)] nanocomposite stands out as a more sustainable alternative. It performs excellently under environmentally friendly conditions, achieving high yields in short reaction times. Moreover, it was synthesized using low-cost, green reagents through a simple and multi-gram scale strategy and shows minimal metal leaching. This makes it a promising, efficient, and eco-friendly option compared to conventional methods (Table 3).

4. Conclusions

In conclusion, a novel nanomagnetic nickel complex was successfully synthesized by a straightforward three-step post-synthesis method. This involved functionalizing Fe_3O_4 magnetic nanoparticles with glycine, converting it to salicylamide, and subsequently complexing with nickel and proline. The resulting material exhibits excellent thermal stability, a high surface area, and a spherical morphology with particle sizes ranging from 14 to 25 nm. This catalyst proved highly effective in the homoselective synthesis of 5-substituted-1*H*-tetrazoles *via* click condensation of various organic nitriles and sodium azide in PEG-400 at 120 °C, affording good to excellent yields (88–99 yield% in 15–85 min). Furthermore, the catalyst demonstrated remarkable reusability, enhanced stability, and minimal leaching. These findings highlight the potential of this catalyst for advancing catalysis, particularly in surface amination using glycine and the immobilization of carboxyl-containing ligands *via* direct amidation. These heterogeneous catalysts hold considerable promise for diverse catalytic applications. Future studies could explore the applicability of this direct amidation method on the catalyst surface for immobilizing carboxylic acid-containing ligands, further enhancing its potential for catalytic applications.

Data availability

The authors declare that all the data are available the data within the paper.

Author contributions

Chou-Yi Hsu: characterization of catalyst. Ghusoon Faidhi Hameed: writing original draft, laboratory works. Abhinav Kumar: conceptualization, analysis, review draft, acquiring research funding and supervision. Subbulakshmi Ganesan and S. Sunitha: laboratory works, catalysis studies and analysis. Irfan Ahmad and Aman Shankhyan: conceptualization, software and review/editing. Rajashree Panigrahi: laboratory works, analysis, review/editing.

Conflicts of interest

The authors declare that they have no competing interests.

Acknowledgements

The authors are thankful to the Deanship of Research and Graduate Studies, King Khalid University, Abha, Saudi Arabia, for financially supporting this work through the Large Research Group Project under grant no. R.G.P.2/516/45.

References

1 L. V. Chanu and O. M. Singh, Recent progress in the synthesis of azoles and related five-membered ring heterocycles using silica-supported heterogeneous catalysts, *J. Heterocycl. Chem.*, 2021, **58**, 2207–2225.

2 L. V. Chanu and O. M. Singh, Recent progress in the synthesis of azoles and related five-membered ring heterocycles using silica-supported heterogeneous catalysts, *J. Heterocycl. Chem.*, 2021, **58**, 2207–2225.
3 J. Revuelta, F. Machetti and S. Cicchi, *Five-Membered Heterocycles: 1,3-Azoles, in Modern Heterocyclic Chemistry*, Wiley, 2011, pp. 809–923.
4 J. Revuelta, F. Machetti and S. Cicchi, Five-Membered Heterocycles: 1,3-Azoles, in *Modern Heterocyclic Chemistry*, ed. J. Alvarez-Builla, J. J. Vaquero and J. Barluenga, Wiley-VCH, Weinheim, 2011, ch. 10, vol. 4, pp. 809–923.
5 A. Rusu, O.-L. Oancea, C. Tanase, *et al.*, Unlocking the Potential of Pyrrole: Recent Advances in New Pyrrole-Containing Compounds with Antibacterial Potential, *Int. J. Mol. Sci.*, 2024, **25**, 12873.
6 P. Solo and D. M. Arockia, Unlocking the imidazole ring: a comprehensive review of synthetic strategies, *Synth. Commun.*, 2025, **55**, 183–235.
7 J. Portilla, Current Advances in Synthesis of Pyrazole Derivatives: An Approach Toward Energetic Materials, *J. Heterocycl. Chem.*, 2024, **61**, 2026–2039.
8 I. Ameziane El Hassani, K. Rouzi, A. Ameziane El Hassani, *et al.*, Recent Developments Towards the Synthesis of Triazole Derivatives: A Review, *Organics*, 2024, **5**, 450–471.
9 M. Lu, P. Wang and Y. Xu, *et al.*, Chemistry of Pentazole, in *Nitrogen-Rich Energetic Materials*, ed. M. Gozin and L. L. Fershtat, Wiley-VCH GmbH, Weinheim, 2022, ch. 1, pp. 1–45.
10 C. G. Neochoritis, T. Zhao and A. Dömling, Tetrazoles *via* Multicomponent Reactions, *Chem. Rev.*, 2019, **119**, 1970–2042.
11 R. E. Trifonov and V. A. Ostrovskii, Tetrazoles and Related Heterocycles as Promising Synthetic Antidiabetic Agents, *Int. J. Mol. Sci.*, 2023, **24**, 17190.
12 M. Nasrollahzadeh, Z. Nezafat, N. S. S. Bidgoli, *et al.*, Use of tetrazoles in catalysis and energetic applications: recent developments, *Mol. Catal.*, 2021, **513**, 111788.
13 G. Aromí, L. A. Barrios, O. Roubeau, *et al.*, Triazoles and tetrazoles: prime ligands to generate remarkable coordination materials, *Coord. Chem. Rev.*, 2011, **255**, 485–546.
14 S. Swami, S. N. Sahu and R. Shrivastava, Nanomaterial catalyzed green synthesis of tetrazoles and its derivatives: a review on recent advancements, *RSC Adv.*, 2021, **11**, 39058–39086.
15 M. A. Gouda, M. Al-Ghorbani, M. H. Helal, *et al.*, A review: recent progress on the synthetic routes to 1(5)-substituted 1*H*-tetrazoles and its analogs, *Synth. Commun.*, 2020, **50**, 3017–3043.
16 D. Ray, A Greener Synthetic Approach to Tetrazoles *via* Multicomponent Reactions, *Curr. Organocatal.*, 2023, **10**, 250–262.
17 Y. Yuan, M. Li, V. Apostolopoulos, *et al.*, Tetrazoles: a multi-potent motif in drug design, *Eur. J. Med. Chem.*, 2024, **279**, 116870.
18 R. J. J. Herr, 5-Substituted-1*H*-tetrazoles as carboxylic acid isosteres: medicinal chemistry and synthetic methods, *Bioorg. Med. Chem.*, 2002, **10**, 3379–3393.
19 A. Maleki and A. Sarvary, Synthesis of tetrazoles *via* isocyanide-based reactions, *RSC Adv.*, 2015, **5**, 60938–60955.
20 M. Schmallegger, M. Wiech, S. Soritz, *et al.*, Polystyrene-bound $AlCl_3$ – a catalyst for the solvent-free synthesis of aryl-substituted tetrazoles, *Catal. Sci. Technol.*, 2025, DOI: **10.1039/D4CY01215A**.
21 R. Mozafari, M. Mohammadi, S. Moradi, *et al.*, In situ synthesis of ultrafine Cu(II) metal immobilized on pectin hydrogel, modified by a $CoFe_2O_4$/Pr-SO_3H nanocomposite as a green catalyst for reduction of nitro compounds and synthesis of 1*H*-tetrazoles, *RSC Adv.*, 2025, **15**, 1358–1374.
22 R. Singh and N. Ahmed, Direct One-Pot Synthesis of Tetrazole Derivatives from Aldehydes under Metal-Free Conditions, *Synlett*, 2024, DOI: **10.1055/a-2493-7974**.
23 M. Khodamorady, N. Ghobadi and K. Bahrami, Homoselective synthesis of 5-substituted 1*H*-tetrazoles and one-pot synthesis of 2,4,5-trisubstuted imidazole compounds using BNPs@SiO2-TPPTSA as a stable and new reusable nanocatalyst, *Appl. Organomet. Chem.*, 2021, **35**, e6144.
24 N. Moeini, M. Ghadermazi and S. Molaei, Synthesis and characterization of magnetic Fe_3O_4@creatinine@Zr nanoparticles as novel catalyst for the synthesis of 5-substituted 1*H*-tetrazoles in water and the selective oxidation of sulfides with classical and ultrasonic methods, *J. Mol. Struct.*, 2022, **1251**, 131982.
25 D. Khalili, R. Evazi, A. Neshat, *et al.*, Copper(I) Complex of Dihydro Bis(2-Mercapto Benzimidazolyl) Borate as an Efficient Homogeneous Catalyst for the Synthesis of 2*H*-Indazoles and 5-Substituted 1*H*-Tetrazoles, *ChemistrySelect*, 2021, **6**, 746–753.
26 M. Valipour, S. Habibzadeh and M. Taherimehr, Synthesis of 5-substituted-1*H*-tetrazoles by lemon juice as a homogeneous and natural catalyst under green reaction conditions, *J. Indian Chem. Soc.*, 2024, **101**, 101382.
27 M. A. Ashraf, Z. Liu, C. Li, *et al.*, Fe_3O_4@L-lysine–Pd(0) organic–inorganic hybrid: as a novel heterogeneous magnetic nanocatalyst for chemo and homoselective [2 + 3] cycloaddition synthesis of 5-substituted 1*H*-tetrazoles, *Appl. Organomet. Chem.*, 2021, **35**, e6133.
28 S. D. Guggilapu, S. K. Prajapti, A. Nagarsenkar, *et al.*, Indium(III) Chloride Catalyzed Synthesis of 5-Substituted 1*H*-Tetrazoles from Oximes and Sodium Azide, *Synlett*, 2016, **27**, 1241–1244.
29 S. Molaei and M. Ghadermazi, Silver complex anchored on ordered mesoporous coated cobalt ferrite nanoparticles as highly reusable catalyst for synthesis of tetrazole, *Appl. Surf. Sci. Adv.*, 2023, **18**, 100519.
30 B. Tahmasbi, P. Moradi and M. Darabi, A new neodymium complex on renewable magnetic biochar nanoparticles as an environmentally friendly, recyclable and efficient nanocatalyst in the homoselective synthesis of tetrazoles, *Nanoscale Adv.*, 2024, **6**, 1932–1944.

31 S. Molaei and M. Ghadermazi, Immobilization of cerium(IV) and erbium(III) in mesoporous MCM-41: two novel and highly active heterogeneous catalysts for the synthesis of 5-substituted tetrazoles, and chemo- and homoselective oxidation of sulfides, *Appl. Organomet. Chem.*, 2019, **33**, e4854.

32 S. Molaei, N. Moeini and M. Ghadermazi, Synthesis of $CoFe_2O_4$@amino glycol/Gd nanocomposite as a high-efficiency and reusable nanocatalyst for green oxidation of sulfides and synthesis of 5-substituted 1*H*-tetrazoles, *J. Organomet. Chem.*, 2022, **977**, 122459.

33 M. Ghadermazi and S. Molaei, Synthesis of Sm(III) complex immobilized in MCM-41: a new heterogeneous catalyst for the facile synthesis of 5-substituted 1*H*-tetrazoles *via* [3 + 2] cycloaddition of nitriles and sodium azide, *Inorg. Chem. Commun.*, 2023, **147**, 110225.

34 S. Naderi, R. Sandaroos, S. Peiman, *et al.*, Synthesis and Characterization of a Novel Crowned Schiff Base Ligand Linked to Ionic Liquid and Application of its Mn(III) Complex in the Epoxidation of Olefins, *Chem. Methodol.*, 2023, **7**, 392–404.

35 A. Nikseresht, F. Ghoochi and M. Mohammadi, Postsynthetic Modification of Amine-Functionalized MIL-101(Cr) Metal–Organic Frameworks with an EDTA-Zn(II) Complex as an Effective Heterogeneous Catalyst for Hantzsch Synthesis of Polyhydroquinolines, *ACS Omega*, 2024, **9**, 28114–28128.

36 M. Mohammadi, M. Khodamorady, B. Tahmasbi, *et al.*, Boehmite nanoparticles as versatile support for organic–inorganic hybrid materials: synthesis, functionalization, and applications in eco-friendly catalysis, *J. Ind. Eng. Chem.*, 2021, **97**, 1–78.

37 Y. Zou, Z. Sun, Q. Wang, *et al.*, Core–Shell Magnetic Particles: Tailored Synthesis and Applications, *Chem. Rev.*, 2024, **125**(2), 972–1048.

38 V. Polshettiwar, R. Luque, A. Fihri, *et al.*, Magnetically recoverable nanocatalysts, *Chem. Rev.*, 2011, **111**, 3036–3075.

39 S. Peiman, B. Maleki and M. Ghani, Fe_3O_4@SiO_2@Mel-Rh-Cu: A High-Performance, Green Catalyst for Efficient Xanthene Synthesis and Its Application for Magnetic Solid Phase Extraction of Diazinon Followed by Its Determination through HPLC-UV, *Chem. Methodol.*, 2024, **8**, 257–279.

40 S. Peiman, B. Maleki and M. Ghani, Fe_3O_4@gC_3N_4@thiamine: a novel heterogeneous catalyst for the synthesis of heterocyclic compounds and microextraction of tebuconazole in food samples, *Sci. Rep.*, 2024, **14**, 21488.

41 S. Peiman and B. Maleki, Fe_3O_4@SiO_2@NTMPThio-Cu: a sustainable and eco-friendly approach for the synthesis of heterocycle derivatives using a novel dendrimer template nanocatalyst, *Sci. Rep.*, 2024, **14**, 17401.

42 S. Peiman, B. Maleki and M. Ghani, Dendrimer templated ionic liquid nanomagnetic for efficient coupling reactions, *Sci. Rep.*, 2024, **14**, 25082.

43 B. Maleki, S. S. Ashrafi, P. G. Kargar, *et al.*, A novel recyclable hydrolyzed nanomagnetic copolymer catalyst for green, and one-pot synthesis of tetrahydrobenzo[*b*]pyrans, *Sci. Rep.*, 2024, **14**, 30940.

44 S. Lotfi, A. Nikseresht and N. Rahimi, Synthesis of Fe_3O_4@SiO_2/isoniazid/Cu(II) magnetic nanocatalyst as a recyclable catalyst for a highly efficient preparation of quinolines in moderate conditions, *Polyhedron*, 2019, **173**, 114148.

45 M. Niakan, P. Ghamari Kargar, B. Maleki, *et al.*, $AgFe_2O_4$@g-C_3N_4@SO_3H Nanocomposite: Efficient and Heterogeneous Photocatalyst for the Production of 5-Hydroxymethylfurfural as a Renewable Biofuel under Visible-Light Irradiation, *Energy Fuels*, 2025, **39**, 1628–1639.

46 P. Ghamari Kargar, B. Maleki and M. Ghani, Ag/GO/Fe_3O_4/γ-Fe_2O_3 Nanocomposite for Green-Light-Driven Photocatalytic Oxidation of 5-Hydroxymethylfurfural to 5-Hydroxymethyl-2-furancarboxylic Acid, *ACS Appl. Nano Mater.*, 2024, **7**, 8765–8782.

47 P. G. Kargar, M. Niakan, B. Maleki, *et al.*, Heterogeneous Photocatalytic Conversion of Biomass-Derived Sugars into 5-Hydroxymethylfurfural over $AgFe_2O_4$/TiO_2-SO_3H Nanocomposite, *ACS Sustainable Chem. Eng.*, 2024, **12**, 18149–18160.

48 H. Veisi, A. Nikseresht, A. Rostami, *et al.*, Fe_3O_4@PEG core/shell nanoparticles as magnetic nanocatalyst for acetylation of amines and alcohols using ultrasound irradiations under solvent-free conditions, *Res. Chem. Intermed.*, 2019, **45**, 507–520.

49 A. Nikseresht, M. Karami and M. Mohammadi, Phosphotungstic Acid-Supported Hercynite: A Magnetic Nanocomposite Catalyst for the Selective Esterification of Chloroacetic Acid, *Langmuir*, 2024, **40**, 18512–18524.

50 Y. Wei, B. Han, X. Hu, *et al.*, Synthesis of Fe_3O_4 nanoparticles and their magnetic properties, *Procedia Eng.*, 2012, **27**, 632–637.

51 G. K. Kharmawlong, R. Nongrum, B. Chhetri, *et al.*, Green and efficient one-pot synthesis of 2,3-dihydroquinazolin-4(1*H*)-ones and their anthelmintic studies, *Synth. Commun.*, 2019, **49**, 2683–2695.

52 I. Dindarloo Inaloo, S. Majnooni, H. Eslahi, *et al.*, Nickel(II) Nanoparticles Immobilized on EDTA-Modified Fe_3O_4@SiO_2 Nanospheres as Efficient and Recyclable Catalysts for Ligand-Free Suzuki–Miyaura Coupling of Aryl Carbamates and Sulfamates, *ACS Omega*, 2020, **5**, 7406–7417.

53 A. Ghasemi-Ghahsareh, J. Safaei-Ghomi and H. S. Oboudatian, Supported l-tryptophan on Fe_3O_4@SiO_2 as an efficient and magnetically separable catalyst for one-pot construction of spiro[indene-2,2′-naphthalene]-4′-carbonitrile derivatives, *RSC Adv.*, 2022, **12**, 1319–1330.

54 R. Foroutan, S. J. Peighambardoust, S. Hemmati, *et al.*, Zn^{2+} removal from the aqueous environment using a polydopamine/hydroxyapatite/Fe_3O_4 magnetic composite under ultrasonic waves, *RSC Adv.*, 2021, **11**, 27309–27321.

55 Z. He, L. Feng, P. Wu, *et al.*, A Top-Down Approach to Synthesis of pH-Controlled Cu NPs: Their Catalytic Activity toward the One-Pot Preparation of α-Aminonitriles and 5-Substituted 1*H*-Tetrazoles from Aldehydes, *ChemistrySelect*, 2020, **5**, 7753–7767.

56 J. Bonnamour and C. Bolm, Iron salts in the catalyzed synthesis of 5-substituted 1*H*-tetrazoles, *Chem.—Eur. J.*, 2009, **15**, 4543–4545.
57 M. Esmaeilpour, J. Javidi and S. Zahmatkesh, One-pot synthesis of 1- and 5-substituted 1*H*-tetrazoles using 1,4-dihydroxyanthraquinone–copper(II) supported on superparamagnetic Fe_3O_4@SiO_2 magnetic porous nanospheres as a recyclable catalyst, *Appl. Organomet. Chem.*, 2016, **30**, 897–904.
58 M. Yadollahi, H. Hamadi and V. Nobakht, Tandem magnetization and post-synthetic metal ion exchange of metal–organic framework: synthesis, characterization and catalytic study, *Appl. Organomet. Chem.*, 2019, **33**(4), e4819.
59 A. M. Liao, T. Wang, B. Cai, *et al.*, Design, synthesis and evaluation of 5-substituted 1-*H*-tetrazoles as potent anticonvulsant agents, *Arch. Pharmacal Res.*, 2017, **40**, 435–443.
60 S. A. Padvi and D. S. Dalal, Choline chloride–$ZnCl_2$: recyclable and efficient deep eutectic solvent for the [2 + 3] cycloaddition reaction of organic nitriles with sodium azide, *Synth. Commun.*, 2017, **47**, 779–787.
61 J. M. McManus and R. M. Herbst, Tetrazole Analogs of Aminobenzoic Acid Derivatives, *J. Org. Chem.*, 1959, **24**, 1044–1046.
62 M. Abdollahi-Alibeik and A. Moaddeli, Multi-component one-pot reaction of aldehyde, hydroxylamine and sodium azide catalyzed by Cu-MCM-41 nanoparticles: a novel method for the synthesis of 5-substituted 1*H*-tetrazole derivatives, *New J. Chem.*, 2015, **39**, 2116–2122.
63 P. Akbarzadeh, N. Koukabi and E. Kolvari, Anchoring of triethanolamine–Cu(II) complex on magnetic carbon nanotube as a promising recyclable catalyst for the synthesis of 5-substituted 1*H*-tetrazoles from aldehydes, *Mol. Diversity*, 2020, **24**, 319–333.
64 N. Nowrouzi, S. Farahi and M. Irajzadeh, 4-(*N*,*N*-Dimethylamino)pyridinium acetate as a recyclable catalyst for the synthesis of 5-substituted-1*H*-tetrazoles, *Tetrahedron Lett.*, 2015, **56**, 739–742.
65 A. Babu and A. Sinha, Catalytic Tetrazole Synthesis *via* [3 + 2] Cycloaddition of NaN_3 to Organonitriles Promoted by Co(II)-complex: Isolation and Characterization of a Co(II)-diazido Intermediate, *ACS Omega*, 2024, **9**, 21626–21636.
66 M. Miceli, P. Frontera, A. Macario, *et al.*, Recovery/reuse of heterogeneous supported spent catalysts, *Catalysts*, 2021, **11**, 591.
67 Z. Du, C. Si, Y. Li, *et al.*, Improved synthesis of 5-substituted 1*H*-tetrazoles *via* the [3 + 2] cycloaddition of nitriles and sodium azide catalyzed by silica sulfuric acid, *Int. J. Mol. Sci.*, 2012, **13**, 4696–4703.
68 M. Norouzi, N. Noormoradi and M. Mohammadi, Nanomagnetic tetraaza (N4 donor) macrocyclic Schiff base complex of copper(ii): synthesis, characterizations, and its catalytic application in Click reactions, *Nanoscale Adv.*, 2023, **5**, 6594–6605.
69 Z. Heidarnezhad, A. Ghorbani-Choghamarani and Z. Taherinia, Magnetically recoverable Fe_3O_4@SiO_2@SBA-3@2-ATP-Cu: an improved catalyst for the synthesis of 5-substituted 1*H*-tetrazoles, *Nanoscale Adv.*, 2024, **6**, 4360–4368.
70 A. Jabbari, P. Moradi and B. Tahmasbi, Synthesis of tetrazoles catalyzed by a new and recoverable nanocatalyst of cobalt on modified boehmite NPs with 1,3-bis(pyridin-3-ylmethyl)thiourea, *RSC Adv.*, 2023, **13**, 8890–8900.
71 M. Nasrollahzadeh, M. Sajjadi, M. R. Tahsili, *et al.*, Synthesis of 1-substituted 1*H*-1,2,3,4-tetrazoles using biosynthesized Ag/sodium borosilicate nanocomposite, *ACS Omega*, 2019, **4**, 8985–9000.
72 S. Kumar, A. Kumar, A. Agarwal, *et al.*, Synthetic application of gold nanoparticles and auric chloride for the synthesis of 5-substituted 1*H*-tetrazoles, *RSC Adv.*, 2015, **5**, 21651–21658.